Next-gen solutions: deep learning-enhanced design of joint cognitive radar and communication systems for noisy channel environments.

MUNIR, M.F., BASIT, A., KHAN, W., SALEEM, A., KHALIQ, A. and BAIG, N.A.

2024

Computers and Electrical Engineering 120 (2024) 109663

Contents lists available at ScienceDirect

Computers and Electrical Engineering

journal homepage: www.elsevier.com/locate/compeleceng

Next-Gen solutions: Deep learning-enhanced design of joint cognitive radar and communication systems for noisy channel environments

Muhammad Fahad Munir [a], Abdul Basit [a], Wasim Khan [a], Ahmed Saleem [a], Aleem Khaliq [a], Nauman Anwar Baig [b,*]

[a] Department of Electrical & Computer Engineering, International Islamic University, Islamabad, 44100, Pakistan
[b] School of Engineering, Robert Gordon University, Aberdeen AB25 1HZ, Scotland, United Kingdom

ARTICLE INFO

Keywords:
CNN based DFRC
DFRC modulation classification
Channel estimation by deep learning
DFRC spectrum efficiency optimization
DFRC cognitive architecture

ABSTRACT

In recent years, the dual-function radar and communication (DFRC) paradigm has emerged as a focal point in addressing spectrum congestion challenges. However, prevailing research heavily relies on computationally complex likelihood-based approaches for communication signals with an added Gaussian noise based single waveform. Note that, a single waveform for diverse scenarios e.g., presence of a communication receiver in the radar main lobe, side lobe, etc., may lead to a deteriorated detection performance in a DFRC design. Therefore, in this paper, we present a cognitive DFRC architecture that utilizes a diverse set of orthogonal waveforms at the transmitter. Specifically, based on a perception-action cycle, a QAM-based waveform is employed for communication when both the radar target and communication receiver are within the main lobe, while a PSK-based waveform is used when the radar target is in the main lobe and the communication receiver is in the side lobes. Furthermore, to enhance the feature-based estimation, the communication receiver integrates a Convolutional Neural Network (CNN) architecture designed to autonomously learn and extract features from received signals with different Signal-to-Noise ratio (SNR). Next, the adaptive nature of the system enables proficient discernment of the received signal type and its corresponding SNR value. Moreover, deep learning techniques are applied in realistic scenarios with various channel impairments to extract features from received signals, departing significantly from likelihood-based methods and reducing computational complexity. The proposed methodology's effectiveness is validated through Monte Carlo simulations, underscoring its potential to address challenges associated with DFRC under real-world conditions.

1. Introduction

Rapid growth in radar-based applications and wireless communicating devices especially 5G and beyond (B5G) desires to increase the bandwidth for better quality of service [1]. It is important to remember that millimeter-waves, multiple-input multiple-output (MIMO), massive MIMO and non-orthogonal multiple access (NOMA) are the key technologies associated with 5G [2–5]. By leveraging these techniques, wireless technologies have the potential to make communication more efficient, reliable, and cost-effective. Wireless technology today aims to reduce hardware and installation costs and maximize radio frequency (RF)

* Corresponding author.
E-mail address: n.baig@rgu.ac.uk (N.A. Baig).

https://doi.org/10.1016/j.compeleceng.2024.109663
Received 13 March 2024; Received in revised form 22 July 2024; Accepted 4 September 2024

spectrum utilization. To satisfy this demand, creative solutions must be developed to optimize the use of the limited radio spectrum resources [6]. Initially, the radio spectrum was allocated to radar-based operations and was used for military purposes only, but with the advent of time, demand in the civilian sector grew exponentially and spectrum scarcity was produced [7]. To overcome this issue, cognitive behavior was adopted to facilitate both entities. Radars were allowed to act as primary users while communication was done as the secondary user under the constraint of power threshold [8]. Several researchers from different parts of the world have been working together to design a unified aperture that can be used for both radar operations as well as communication functions. Through this joint architecture, communication users are provided with a share of the bandwidth originally allocated to radar operations [9].

Generally, spectrum sharing can be done in the time domain or the spectral domain [7]. In the time domain, a strobe switch is used for switching while the spectral coexistence is further divided into two broad fields: Joint radar and communications (JRC) and dual function radar and communications (DFRC) [10]. In JRC both entities share spectrum only while in DFRC, the unified transmitter is used for both radar and communication operations. DFRC utilizes three different categories of waveforms. These waveforms are radar-based waveform design, communication-derived waveform design, and the sub-beam approach [11]. The Radars and wireless devices can share spectrum and hardware simultaneously using the DFRC approach. This technology maximizes spectrum efficiency by reducing the need for a dedicated spectrum for each service, thereby allowing more users to access the spectrum [12,13]. There has been considerable interest in the subject of spectrum congestion among researchers. Nevertheless, two broad categories of algorithms can be applied to received signals: likelihood-based (LB) and feature-based (FB). The first category applies spectral densities (PSD), calculating the probabilities ratio between the signals and applying matched filtering-related techniques, whereas, in the second category, features are extracted from the received signal and used to make a decision. The results of the LB-based approach are reliable, provide us optimal solution but the computation complexity is high. In contrast, the FB approach is easy to implement and gives us the freedom to ignore transmission schemes and the nature of devices. Furthermore, they are robust enough to take account of channel mismatches.

1.1. Likelihood based estimation

Likelihood-based detection is one type of spectrum-sharing solution as explained above. It uses the likelihood of a signal received by a communication user determined by its channel impairments such as noise, fading and other distortions to estimate whether that signal belongs to another spectrum user or not [14]. The approaches used in likelihood-based detection include calculating conditional probabilities through Bayesian modeling, using pattern recognition techniques, and involving artificial intelligence algorithms like neural networks [15–17]. LB offers a high degree of accuracy in detecting spectrum signals from other spectrum users without introducing any false alarms or miss-detections [18]. Also, they can detect low-power signals amidst strong interference. Furthermore, they can also reject narrowband interference and identify multiple users transmitting simultaneously with different modulations [19]. Spectrum-sharing systems benefit significantly from advanced detectors, leading to enhanced accuracy. Likelihood-based detectors' performance relies on various factors including signal-to-noise ratio, the number of available samples per interval, and the number of modulation types [20].

To achieve more efficient and secure transmission, researchers propose using amplitude shift keying to embed information for communication receivers positioned in sidelobes of radar beams [21]. ASK modulation has performance constraints and lower bit rates when the radar and communication receivers are positioned in the main lobe. This technique suffers from reduced performance and bit rate. [22]. To address this issue, a PSK-based technique has been proposed in [23]. This approach performs well when the communication receiver is positioned within the main lobe of the radar beam. Moreover, recent research [24] suggests that utilizing a quadrature amplitude modulation (QAM)-based approach for information embedding yields improved performance compared to existing ASK methods based on sidelobe level (SLL), waveform diversity, and PSK. Additionally, insights provided by [9] delve into likelihood-based estimation techniques and various information-embedding strategies.

1.2. Feature based estimation

The feature-based estimation technique extracts multiple features from the received signal to estimate the characteristics of the transmitted signal, such as its range, velocity, amplitude, phase frequency, and modulation type [25]. By using FB estimation techniques, cognitive radio systems can determine if a signal is legitimate and thus help prevent false alarm detection [26]. Ultimately, FB estimation is essential for reliable spectrum sharing and efficient cognitive radio networks. Additionally, with improved communications performance and efficient spectrum exploitation, FB estimation can provide a valuable tool for interference avoidance in wireless networks [27]. The FB classification can be implemented by Combining with Kalman Filtering [28] or Hidden Markov Models (HMM) to improve the efficacy of results and prevent false detections [29].

The sub-optimal Feature-based method is developed to classify signals by identifying useful features before the classification process [30]. These features can include instantaneously calculated values, transformed representations, statistical measures, or characteristics derived from constellation shapes. Extensive research has been conducted on both methods, revealing that the LB method offers the most effective solution but demands significant computational resources and prior knowledge of the signal. On the other hand, although less optimal in terms of accuracy, the FB method provides a faster response time due to its lack of dependence on prior information. In ML-based techniques, feature extraction becomes a task requiring expertise when employing these methods [31]. To overcome this challenge in FB methods and enhance their efficacy in recognizing complex patterns effectively compared to shallow models do deep learning approaches have drawn considerable attention for reducing reliance on traditional

feature engineering methodologies. Due to the rapid advancements in DL technologies, numerous methods have been developed to self-learn the features, and DL is preferred because it requires large datasets, which are easily obtained from communication systems. The complexity of DL is a major concern since it involves training and testing phases, many applications have utilized depthwise convolutional networks. As a result of depth-wise convolutions, the model size is reduced significantly, but accuracy remains the same. Compared to conventional convolution, this model has fewer parameters, making it suitable for small devices in cognitive environments. In [32], authors applied a Markov-based decision process and Deep Q network to estimate the target parameters for cognitive radar. The main achievement is to minimize the interference between radar and the communication user. In [31] separable convolutional neural network (CNN) is applied to estimate features of the received signal at the communication receiver. The authors have applied CNN architecture to the signal received from a highly noise-impaired channel. Similarly, in [33] long short-term memory (LSTM) with a gated recurrent unit (GRU) layer is applied to obtain higher accuracy for B5G wireless networks and Internet of Things (IoT) networks. The efficacy of results is measured in terms of accuracy, training loss, and confusion matrix. The value of the SNR is used between −20 dB to 20 dB. A few more models based on CNN architectures are studied in [34–36] mainly focusing on the extraction of features and calculating the computational complexity and accuracy of proposed models. In [37,38], researchers skipped the features extraction step to further reduce the computational complexities. Similarly, to increase the performance while keeping low computational complexities, the combination of CNN with recurrent neural network (RNN) is presented in [39,40]. More details about the use of CNN, RNN, and other variants of DL algorithms have been widely discussed in literature by [41,42].

In this investigation, we introduce a methodology that employs multiple orthogonal waveforms for information embedding, encompassing the following key aspects:

- Diverse Waveform Usage: A QAM-based waveform is chosen for communication when both the radar target and the communication receiver are positioned within the main lobe. Alternatively, a PSK-based waveform is employed when the radar target is within the main lobe and the communication receiver is situated in the side lobes.
- CNN-Based Feature Extraction: The CNN-based architecture presented in this study is meticulously designed to autonomously learn and extract features from received signals characterized by a specified SNR.
- Cognitive System Capabilities: This proposed cognitive system (based on the perception-action cycle) proficiently identifies both the type of received signal and its corresponding SNR value. Additionally, these acquired statistics are subsequently communicated to the DFRC fusion center through the communication receiver's uplink.

The subsequent sections of this paper follow a structured arrangement. Section 2 provides insights into the conventional data model. Section 2 details the proposed architecture for Dual-Function Radar and Communication (DFRC). This section covers the discussion on the suggested information embedding methodology at the transmitter side, and the design aspects of both the radar receiver and the communication receiver. Additionally, a thorough examination of the deep learning-based architecture is presented, elucidating detailed information on the path leading to information decoding. Section 3 is dedicated to the presentation and discussion of results, while Section 4 discusses the conclusion, presenting a synthesis of key findings and conclusive remarks drawn from the research.

2. The proposed architecture

Consider the DFRC transmitter with a uniform linear array spaced half the wavelength. The radar receiver is placed adjacent to the DFRC transmitter so that both the DFRC transmitter and the radar receiver observe the same spatial angle. Moreover, We have one communication receiver equipped with both a transmitter array and a receiver array. The DFRC transmitter and the radar receiver contain M_T and M_R antenna elements, while the communication receiver contains N_T and N_R antenna elements in transmitter and receiver arrays respectively. The receiver array at the communication receiver is employed to receive signals from the DFRC transmitter. Meanwhile, the transmitter array at the communication receiver facilitates sending feedback to the fusion center as shown in Fig. 1 and discussed in [13].

The main aim of this data model is to develop a cognition between the DFRC transmitter and the communication receiver. There are two types of feedback received at the fusion center, the first feedback contains the geographical information of the target i.e. angle of arrival and SNR while the information of data will be obtained from the communication as shown in Fig. 2. The objective of the communication uplink path is to provide the knowledge of the channel state information.

The DFRC transmitter generates an omnidirectional waveform that strikes both the target and the communication receiver. The signal strikes back from both the radar receiver and the communication receiver which may or may not be partially overlapped. Further, the communication receiver scans the entire environment and obtains the locations of the target and DFRC transmitter. The communication receiver sends the channel information to the DFRC receiver via the uplink path. Once the channel information is updated, the fusion center designs the DFRC transmit beamformer. When the target lies in the main lobe and the communication receiver lies in the side lobes, a QAM-based waveform will be used. Similarly, when both the target and communication receiver exist in the main lobe, a PSK-based waveform will be used.

More details about the radar and communication feedback processor are discussed in the communication receiver section. The entire activity is summarized in the following algorithm (see Table 1).

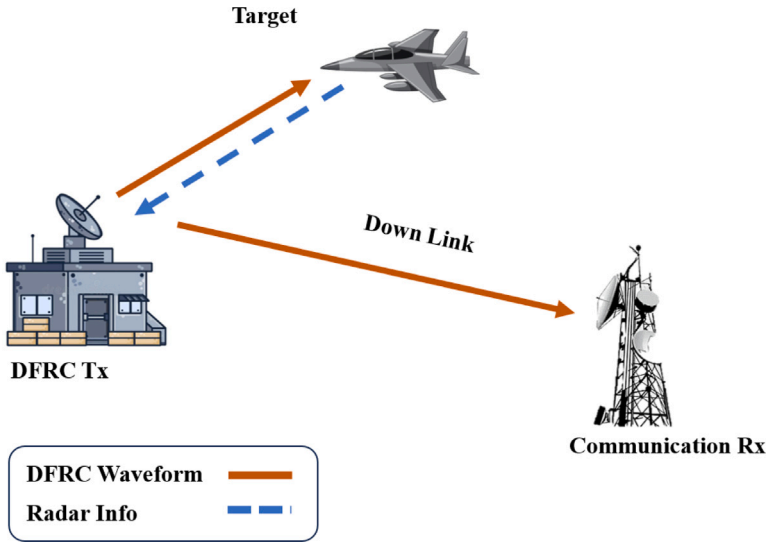

Fig. 1. Data model of existing DFRC [13].

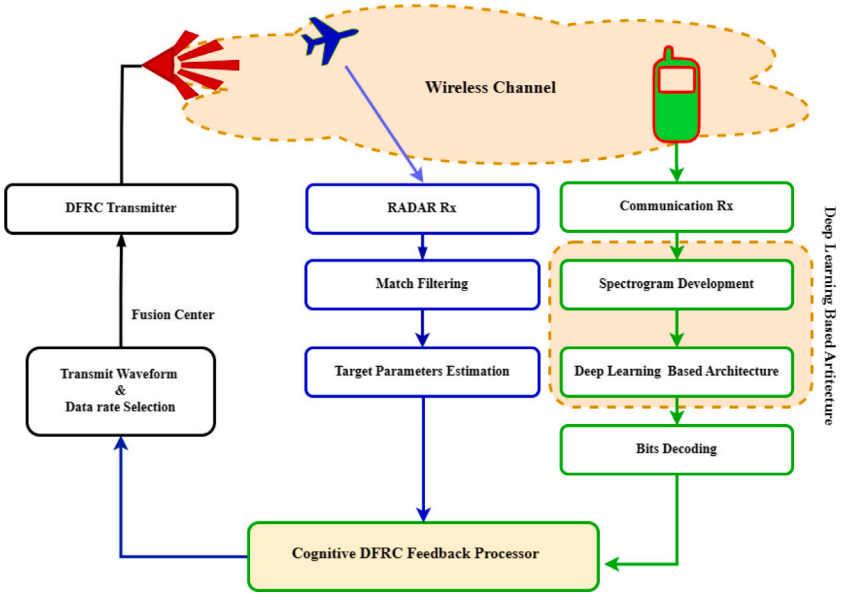

Fig. 2. Flowchart of proposed System.

2.1. DFRC transmitter design

In Fig. 2, the initial module under discussion is the DFRC transmitter. The signal transmitted undergoes channel impairments and interacts with the target in the far-field, as well as the communication receiver. Subsequent sections develop a signal data model for the DFRC design, employing various modulation schemes. DFRC transmitters, radar receivers, and communication receivers are all equipped with uniform linear arrays (ULAs) utilizing M_T, M_R, N_T, and N_R antenna elements, respectively, for the transmission and reception of various signals. The spacing between each element in an array is generally half a wavelength, consistent across all arrays. It is assumed that the DFRC transmitter and radar receiver are positioned so closely that they receive the same angle of radiation. Detection and tracking of radar targets are primarily achieved with the transmitter array. Additionally, the transmitter array encapsulates communication bits without affecting radar operation. DFRC transmitting arrays steer power within the main beam, where radars operate, using this beam of radiation for object detection and location. The radar receiver then interprets the received signal, enabling the user to determine the object's location. At the input of the transmit antenna, the $M_T \times 1$ vector form

Table 1
Radar target search and communication channel estimation.

Algorithm:	Radar target search and communication channel estimation.
Step 1:	DFRC transmitter generates omnidirectional signal to search the target and communication receiver.
Step 2:	Radar receiver receives the echo from target and estimates its angle and reflection coefficients.
Step 3:	Communication receiver estimates the location of DFRC transmitter and target by using the MUSIC algorithm.
Step 4:	Communication receiver decodes the information received in step 2 and sends feedback to DFRC transmitter via Uplink.
Step 5:	DFRC receives the feedback from communication receiver and updates the waveform according to channel behavior.

Table 2
List of symbols.

Symbol	Dimensions	Description
$\psi_1(t)$	$M_T \times 1$	PSK based waveform
$\psi_2(t)$	$M_T \times 1$	QAM based waveform
$g(t)$	1×1	Pulse shaping filter
A_I	1×1	QAM amplitude information In phase
A_Q	1×1	QAM amplitude information Quadrature
t	1×1	Time period of each radar pulse
τ	1×1	Pulse number
A	1×1	Power assigned to each waveform
$\mathbf{w}$	$M_T \times 1$	Beamforming weights
$(\cdot)^*$	$M_T \times 1$	Complex conjugate operator
$\psi(t)$	$M_T \times 1$	Orthogonal waveform
δ	1×1	Kroneker delta
$\mathbf{h}(t)$	$N_R \times 1$	Channel impulse response
$(*)$	1×1	Convolutional operator
$\mathbf{n}(t)$	$M_R \times 1$	The AWG noise vector
A_p	1×1	Received signal power
β_p	1×1	Reflection coefficient
$\mathbf{a}(\theta_p)$	$M_T \times 1$	Transmitter steering vector
θ_p	1×1	Direction of radar target
$\mathbf{s}(t,\tau)$	$M_T \times 1$	Transmitted baseband signal
$\mathbf{b}(\theta_p)$	$M_R \times 1$	Receiver array steering vector
$\mathbf{e}_r(t,\tau)$	$M_R \times 1$	Interference encountered at the radar receiver
$\mathbf{n}_r(t,\tau)$	$M_R \times 1$	Additive white Gaussian noise
d	1×1	Inter element spacing
λ	1×1	Wavelength

of the baseband signal for the τ^{th} pulse is

$$\mathbf{s}(t,\tau) = \mathbf{s}_{radar}(t,\tau) + \mathbf{s}_{com}(t,\tau) \tag{1}$$

In this formula, the signal transmitted from DFRC contains the information of both the radar signal and communication signal.

2.2. Proposed information embedding methodology

Transmitted signals encapsulate binary data conveyed through waveform characteristics, encompassing amplitude, phase, and frequency. Both radar and communication receivers intercept these signals emanating from the DFRC transmitter. The radar receiver employs the MUSIC algorithm to ascertain the object's directional information, whereas the communication receiver deciphers the symbolic information using CNN. On the transmitter side, a single symbol is transmitted within each pulse repetition interval. The choice of this symbol may vary from pulse to pulse, contingent upon the characteristics of the channel. The lookup table comprises numerous waveforms and diverse modulation schemes, including BPSK, QPSK, 8 PSK, 16 QAM, and 64 QAM. Subsequently, the transmitter selects a singular symbol from the assortment of available options for modulation, as illustrated in Fig. 3. The communication receiver identifies the modulation scheme and corresponding waveform, facilitating the extraction of binary information. The list of abbreviations used in this manuscript is mentioned in the below Table 2.

It is important to note that we have to use such orthogonal waveforms whose time-bandwidth product is large. Such waveform gives maximum detectable range and better resolution. The generalized waveform of $M-aryPSK$ and $M-aryQAM$ modulated

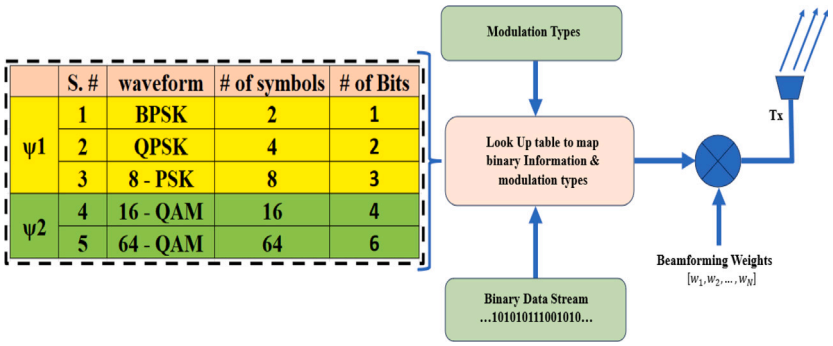

Fig. 3. The proposed information embedding methodology at the DFRC transmitter.

signal is represented by [43]:

$$\psi_{1,j}(t) = g(t)cos(2\pi f_c t + \theta_j)$$
$$\theta_j = \frac{2\pi}{J}(j-1), j = 1, \ldots, J. \tag{2}$$

$$\psi_{2,j}(t) = A_I g(t)cos(2\pi f_c t + \theta_j) - A_Q g(t)sin(2\pi f_c t + \theta_j)$$
$$\theta_j = \frac{2\pi}{J}(j-1), j = 1, \ldots, J. \tag{3}$$

As depicted in Fig. 3, the value of J for PSK-based waveforms is $2, 4, 8$ and for QAM-based waveforms, it is 16 and 64. Thus, at the input of the DFRC transmitter, the combined form of the signals is given by [44]

$$\mathbf{s}(t, \tau) = A(\tau)\mathbf{w}^* \psi(t) \tag{4}$$

The orthogonality of waveform can be written as:

$$\int_t |\psi(t)|^2 \, dt = 1 \tag{5}$$

and

$$\int_t \psi_k \psi_k^*(t) dt = \delta(k - k') \tag{6}$$

where δ is kroneker delta.

Training data is transmitted over a multi-tap rician wireless channel after modulation. The signal passed through the wireless channel looks like

$$\mathbf{r}(t) = \mathbf{s}(t) * \mathbf{h}(t) + \mathbf{n}(t), \tag{7}$$

In matrix-vector form

$$\mathbf{r}(t) = \mathbf{Hs} + \mathbf{n}(t), \tag{8}$$

where $\mathbf{H} = diag(\mathbf{h})$ with $\mathbf{h} = [h_1, h_2, \ldots, h_{M_R}]^T$ is $M_R \times 1$ vector containing channel information and $\mathbf{s} = [s_1, s_2, \ldots, s_{M_R}]^T$ contains the information in the form of amplitudes and phases. Furthermore, due to the multipath channel effect, the complexities of the received signal in Eq. (7) increases as expressed mathematically,

$$r(t) = (s(t - \Delta t) * \sum_{i=1}^{N} \rho_i \delta(t - t_i) e^{j(\phi_i + \Delta\phi)})$$
$$e^{j2\pi\Delta f t} + n(t) \tag{9}$$

where, $s(t - \Delta t)$ accounts for timing offset, $e^{j(\phi_i + \Delta\phi)}$ represents the phase offset added to each multipath component and $e^{j2\pi\Delta f t}$ accounts for the frequency offset. Moreover, $\sum_{i=1}^{N} \rho_i \cdot \delta(t - t_i) \cdot e^{j(\phi_i + \Delta\phi)}$ represents the multipath channel response with N multipath components. Each component includes a delay (t_i), complex attenuation (ρ_i), and phase shift (ϕ_i). These offsets are all introduced simultaneously, and their specific values will depend on the impairments introduced by the channel or other factors in the communication system. Consequently, as a result, the constellation image looks messy due to these channel-introduced impairments, which result in overlapping points. In such constellation images, it is extremely difficult to determine whether the modulation scheme selected is right or wrong.

2.3. Radar receiver design

Suppose there are P distant targets within the radar's main beam. The baseband signal received by the radar receiver can be represented in vector form as follows:

$$\mathbf{x}_{radar}(t,\tau) = A_p \sum_{p=1}^{P} \beta_p(\mathbf{a}^T(\theta_p)\mathbf{s}(t,\tau))\mathbf{b}(\theta_p) + \mathbf{e}_r(t,\tau) + \mathbf{n}_r(t,\tau) \tag{10}$$

The steering vector for the radar receiver array can be written as

$$\mathbf{b}(\theta_p) = [1, e^{j\frac{2\pi}{\lambda}d\sin(\theta_p)}, \ldots, e^{j\frac{2\pi}{\lambda}d(M_R-1)\sin(\theta_p)}]^T \tag{11}$$

For enhanced clarity, Table 2 provides a thorough list of symbols, including their corresponding dimensions and descriptive explanations for Eqs. (10) and (11).

2.4. Communication receiver design

In the far field, there exist J communication receivers, each equipped with N_T and N_R antenna elements for uplink and downlink purposes. To facilitate prior communication, a lookup table containing the dictionary of orthogonal symbols at the dual-function transmitter is known to each communication receiver. The proposed system extracts SNR information from the received signal and subsequently transmits it back to the DFRC transmitter via an uplink antenna array. In literature, this technique is recognized as uplink channel estimation [45]. Assuming that the jth communication receiver, furnished with N_R antenna elements arranged uniformly in a linear configuration, receives the following signal.

$$\mathbf{x}_{com}(t,\tau) = A_j\alpha_j(\mathbf{a}^T(\phi_j)\mathbf{s}(t,\tau))\mathbf{c}_j(\phi_j) + \mathbf{n}_j(t,\tau) \tag{12}$$

The received power at the communication receiver is denoted by A_j. The parameter α_j represents the constant channel coefficient originating from the transmitter array towards the jth communication receiver, summarizing the propagation characteristics. On the other hand, $\mathbf{a}(\phi_j)$ corresponds to the steering vector in the direction of θ_j for the communication receiver from the dual-function transmitter. Moreover, $\mathbf{s}(t,\tau)$ represents the baseband signal carrying actual information. The $\mathbf{c}_j(\phi_j)$ characterizes the steering vector from the receive array, which is related to the communication receiver's location. The noise component $\mathbf{n}_j(t,\tau)$ is an additive white Gaussian noise vector with a zero mean and variance $\sigma^2\mathbf{I}$. Furthermore, (ϕ_j) designates the direction associated with the kth communication receiver.

The steering vector of communication receiver ULA can be written as

$$\mathbf{c}(\theta) = [1, e^{j\frac{2\pi}{\lambda}d\sin(\theta_j)}, \ldots, e^{j\frac{2\pi}{\lambda}d(N_R-1)\sin(\theta_j)}]^T \tag{13}$$

In the initial stage, beamforming is applied to the received signal. This operation isolates the steering vector by employing beamforming weights at the communication receiver. Consequently, the desired signal can be extracted from the received signal, allowing the receiver to focus on the desired signal's direction while mitigating interference from other directions. This reduction in interference enhances the signal-to-noise ratio (SNR) at the receiver. The beam-forming operation is mathematically expressed by Eq. (12). The received signal is comprehensive and contains information on received power, channel impairments, noise, and modulation scheme. These parameters have both deterministic and stochastic nature. More details about the signal parameters are shown below:

$$\mathbf{x}_{com}(t) = \hat{A}e^{j(2\pi\Delta f t+\phi_j)}\eta^{k,i}g(t-nT_s) \tag{14}$$

The amplitude, phase offset, and residual of carrier frequency are represented by $\hat{A}$, ϕ_j, and Δf, whereas symbol interval is written as T_s and g(t) is the pulse shaping. $\eta^{k,i}$ is the modulated symbol with kth waveform and ith constellation.

2.4.1. Spectrogram image diagrams

A spectrogram is a visual representation of the frequencies present in a signal over time. To generate a spectrogram image, a time-domain signal received in Eq. (14) is used. The process involves converting the time-domain signals into frequency-time representations by short-term Fourier transform (STFT), which can then be fed into a neural network for classification. To analyze the signal over short time intervals, the signal is multiplied by a window function. Common window functions include the Hamming window or Gaussian window. The windowed signal is denoted as $x_w(t)$

$$\mathbf{x}_w(t) = \mathbf{x}_{com} \cdot \mathbf{w}(t) \tag{15}$$

Furthermore, the windowed signal is sampled down and FFT is applied on it as

$$\mathbf{X}_d = FFT\{\mathbf{x}_w[n]\} \tag{16}$$

$\mathbf{X}_d$ represents the complex spectrum matrix of the signal at a given frequency. The spectrogram can be mathematically described as a $2D$ matrix:

$$\mathbf{S}(t,f) = |\mathbf{X}_d(f,t)|^2 \tag{17}$$

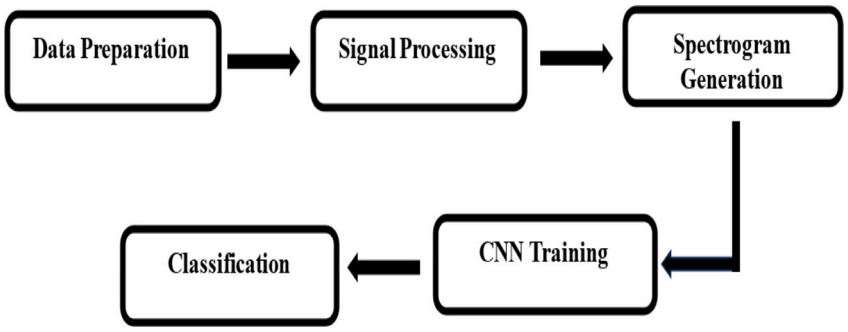

Fig. 4. Flowchart of paper.

Fig. 5. The proposed layered wise CNN architecture.

where, $\mathbf{S}(t, f)$ represents the magnitude of the spectral content at time t and frequency f.

It is worth noting that the implementation of neural networks varies depending on the complexity of the modulation schemes and the size of the dataset. The main objective of using CNN-based architecture is to recognize the unique spectral patterns and temporal characteristics associated with different modulation schemes, enabling it to classify unknown modulation signals accurately.

2.4.2. Proposed convolutional neural network design

In our proposed method, data is effectively classified with the assistance of CNNs. Unlike other classification algorithms, CNNs do not necessitate extensive pre-processing. Convolutional architectures are available in both 2D and 3D, depending on the user's requirements. The structure comprises four layers. The first layer is the convolution layer, responsible for receiving input data and extracting features. This layer performs the convolution operation between the filter and the input map. The second layer is a pooling layer, which reduces the dimensionality of the feature map. Compressing the output of the convolution layer is sometimes necessary, and pooling achieves this by down-sampling the feature map. This enhances feature robustness when there are positional changes. Common methods for pooling include average pooling and maximum pooling. The third layer is fully connected, and tasked with classifying the data. Every neuron in each layer is connected with specific weights and activations to the neurons in the layer above. The fourth layer is the output layer, which delivers the final result. An activation function is utilized to calculate the probability response at the output layer. The overall flow chart of the study is illustrated in Fig. 4.

The CNN architecture is improved by incorporating a fully connected layer and a Softmax classifier layer to enhance its effectiveness. We optimized the hyperparameters for the proposed CNN including learning rate, dropout rate, filter size, number of filters, and network width mentioned in the Tables 5 and 6 respectively. The proposed network, illustrated in Fig. 5, takes spectrogram images as input with dimensions of $1 \times 1024 \times 3$.

A variety of spatial filters, each with several learnable parameters, are employed in the convolutional layers of the proposed design. This facilitates the efficient and rapid learning of spatial properties and other pertinent high-level features. In each convolutional layer, the input undergoes convolution with the filters and is subsequently passed through activation functions. The mathematical description of a the convolutional layer is as follows:

$$\mathbf{G}_{conv} = \zeta(\mathbf{S} \cdot \mathbf{K} + b_{conv}), \tag{18}$$

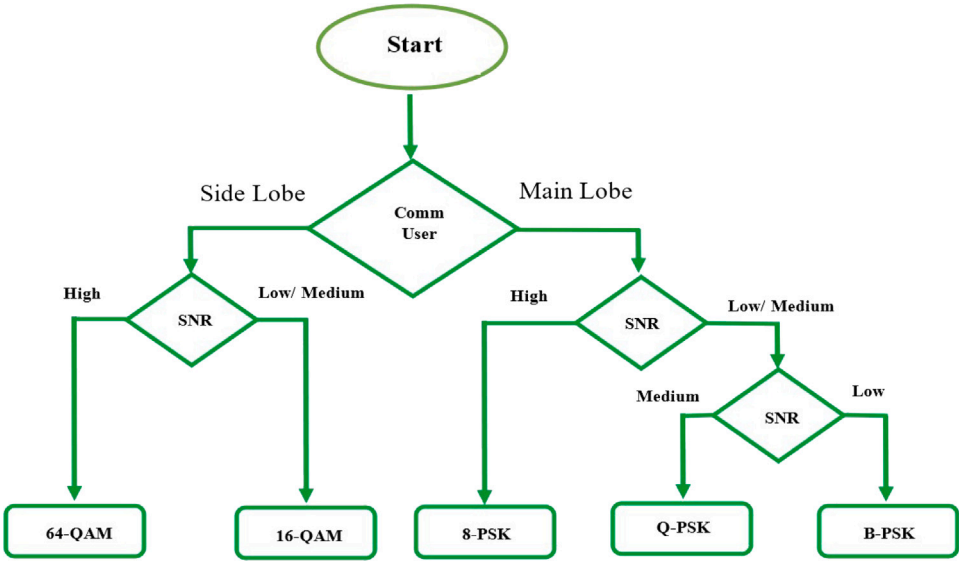

Fig. 6. The internal mechanism of proposed radar and communication feedback processor.

where, ζ is the activation function, **K** is Convolutional layer kernel matrix, **S** is the raw output images obtained by spectrogram and b_{conv} is the bias of for symbol decoding. Furthermore, the samples extracted from convolutional layers are fed to pooling layer for dimensions reduction and feature extraction. The output of the pooling layer can be written as:

$$\mathbf{D}_{pooling} = \daleth(\mathbf{G}_{conv} + b_{pooling}) \tag{19}$$

in Eq. (19), $\daleth$ represents the pooling layer activation function. There are three different types of pooling operations available, i.e. max pooling, average pooling, and $L2-Norm$ pooling. Furthermore, a fully connected layer is responsible for detection of data and it gives us the final answer. Max pooling takes the maximum value within each pooling window, helping to retain the most significant features. furthermore, when dealing with multi-class classification problems, the softmax activation function is applied element-wise to the output vector **D** obtained after the pooling layer. Given an input vector z, the softmax function is defined as:

$$\mathbf{z}_{output} = Softmax(\mathbf{D}) \tag{20}$$

The output of the softmax function is a probability distribution over the classes, and it is commonly used in the final layer of a neural network for classification tasks.

2.5. Proposed cognitive design and adaptive modulation

The design and implementation of a cognitive communication system with adaptive modulation and SNR thresholding present a sophisticated approach to addressing the dynamic nature of communication channels. The system incorporates a cognitive feedback loop that continuously monitors key parameters, such as SNR, channel quality, and interference levels, through a dedicated sensing module. This real-time feedback informs an intelligent decision-making algorithm, enabling the system to dynamically adjust its configuration based on changing channel conditions. The integration of SNR thresholding establishes predefined thresholds for different modulation schemes ($M-PSK\&M-QAM$), allowing the system to select the most suitable modulation scheme at any given moment. This ensures optimal utilization of available bandwidth while balancing the trade-off between data rate and reliability. The adaptive modulation module seamlessly switches between modulation schemes based on the determined SNR thresholds, while rate adaptation mechanisms adjust data rates accordingly. Thorough testing and optimization are essential to fine-tune the system's parameters, ensuring robust performance across diverse communication scenarios. This cognitive communication system represents a sophisticated and dynamic solution for addressing the challenges posed by variable channel conditions. Fig. 6 embodies the selection of waveform and data rate based upon the channel statistics and value of SNR.

The SNR thresholding for the communication receiver to be in the main lobe and in the side lobes are given in Table 3.

2.6. UP link communication channel

Similarly, the signal generated by the communication receiver and transmitted by using ULA having dimension $N_T \times 1$ towards DFRC transmitter or fusion center can be written as:

$$\mathbf{s}_{UL}(t,\tau) = A_{UL}(\tau)\mathbf{w}^*_{UL}\psi_{UL}(t) \tag{21}$$

Table 3
SNR threshold for main lobe and side lobes.

Main lobe		Side lobes	
−15 dB to −5 dB	BPSK	−15 dB to 5 dB	16 QAM
−5 dB to 5 dB	QPSK		
5 dB to 15 dB	8 PSK	5 dB to 15 dB	64 QAM
15 dB and above	16 PSK		

Table 4
Wireless channel parameters.

Parameter name	Parameter value
Modulation schemes	5
Samples of each modulation	1000
Signal dimension	$1 \times 1024 \times 3$
Duration of each input frame	5 ms
Center frequency	902 MHz
SNR range	−30 dB to +30 dB
Sampling rate	200 kHz
Symbols of each waveform	1024
Samples per symbol	8
Doppler spread	5 Hz
Maximum clock offset	5 ppm
Channel profile	Rician
Fading K factor	4
Fading delay ratio	$0, 1.8, 3.4$
Path gains	$0, -2, -10$ dB
Maximum doppler shift	4

where, A_{UL} is the signal power, $\mathbf{w}_{UL}$ is the UL steering vector from the communication receiver towards the DFRC transmitter and $\psi_{UL}(t)$ is the desired waveform contains snr level information.

3. Simulation results

For any learning task, a recommended initial step involves plotting the input data to identify prominent features. If a clear direction is discernible through visualization, utilizing a neural network may be excessive or even sub optimal. To generate the constellation diagram, the receiver must precisely recover the timing, carrier frequency, phase, and waveform of the received signal. Communications systems cannot eliminate channel effects due to their inherent nondeterministic nature. In real-time communication scenarios, factors such as increased thermal noise, oscillator drift and temperature variations at the DFRC transmitter, and symbol timing offset may arise. Additionally, issues such as sample rate degradation and carrier frequency offsets contribute to performance deterioration. Owing to these impairments, accurately identifying the true modulation and transmitted symbol becomes exceedingly challenging.

Furthermore, the presence of multipath fading further degrades signal quality, resulting in data loss. This data loss subsequently exacerbates the performance degradation of the transmission system. The more details about the channel parameters are provided in the Table 4.

In this received signal classification task, at the receiver, 1000 received samples were collected to make a spectrogram diagram in image format by applying short-term Fourier transform (STFT). The generated image is then fed to CNN based classifier for classification. The classification result is a probability vector that indicates the probability of the received constellation being a particular modulation scheme.

In the next section, we present the performance of the proposed CNN-based system. The proposed system has been evaluated based on classification accuracy and miss classification error over a wide range of SNRs.

3.1. Proposed CNN classification performance

In the subsequent section, we will examine the CNN-based received signal classifier, its constellation diagram, and the training procedure. Throughout the CNN training process, various parameters of the optimizer and training algorithm require adjustment to enhance both the training speed and classification accuracy. Specifically, we adopted batch processing during training, employing batches of $10,000$ images for each iteration. To facilitate effective learning, the CNN underwent training for 1000 iterations. Additional details regarding the diverse training parameters of the CNN are provided in Table 5.

Training was done on a standard Intel 11th Gen Intel(R) Core(TM) $i5$ $1135G7$, with 2.40 GHz and 2.42 GHz processors, having 8 GB ram and Intel Iris Xe Graphics $G780EUs$(400–1300 MHz) GPU cards that took 3 h 10 min approximately.

The details of the CNN network layer parameters are comprehensively discussed in Table 6. This encompasses essential information, including the filter size and the number of filters utilized in each layer. Subsequently, each convolutional layer is

Table 5
CNN parameters.

Parameter name	Parameter value
Percent training samples	80%
Percent validation samples	10%
Percent test samples	10%
Mini batch size	10
Initial learning rate	0.0001
Iteration per epoch	500
Validation frequency	3
Max epochs	10
Solver name	Adam

Table 6
CNN layers details.

Layers name	Layer dimensions	Filter size	No. of filters
Input layer	$1 \times 1024 \times 3$		
Conv. layer 1	$1 \times 1024 \times 32$	3×3	32
Conv. layer 2	$1 \times 512 \times 32$	3×3	32
Conv. layer 3	$1 \times 256 \times 32$	3×3	32
Conv. layer 4	$1 \times 128 \times 48$	1×8	48
Conv. layer 5	$1 \times 64 \times 64$	1×8	64
Conv. layer 6	$1 \times 32 \times 96$	1×8	96
Average pooling layer	$1 \times 1 \times 96$	1×1	01
Fully connected layer	$1 \times 1 \times 5$	5	
Softmax layer	$1 \times 1 \times 5$		
Class output layer	$1 \times 1 \times 5$		

Table 7
Confusion matrix of proposed CNN at snr −7 dB.

16 QAM	82	17	1	0	0	82%
64 QAM	14	84	1	0	1	84%
8 PSK	3	1	76	0	20	76%
QPSK	6	0	8	0	86	86%
BPSK	0	0	0	0	100	100%
	16 QAM	64 QAM	8 PSK	QPSK	BPSK	Accuracy (%)

Table 8
Confusion matrix of proposed CNN at snr 0 dB.

16 QAM	92	6	0	0	2	94%
64 QAM	1	91	0	8	0	91%
8 PSK	4	0	94	0	2	94%
QPSK	1	0	1	0	98	98%
BPSK	0	0	0	0	100	100%
	16 QAM	64 QAM	8 PSK	QPSK	BPSK	Accuracy (%)

succeeded by a batch normalization layer, followed by a Rectified Linear Unit (ReLU) activation function and a Max pooling layer. This proposed architectural configuration is designed to enhance training speed, promote better generalization, and yield improved performance.

The results in Table 7 show performance accuracy at −7 dB using a confusion matrix. These values show that for lower SNR values, the modulation accuracy of less data rate is very high.

The accuracy of BPSK at 0 dB is 100% while the classification accuracy of higher modulation order degrades slightly. This degradation occurs due same constellation diagrams. The overall accuracy of the proposed system is 92.6%. To mitigate the risk of encountering local minima, the ADAM optimization algorithm is employed for training the Convolutional Neural Network (CNN). The advantages of Adam over stochastic gradient descent (SGD) extend to improved computational complexities and the calculation of both mean and central variance for the moving average of each parameter. In conjunction with the softmax layer, a cross-entropy loss function is utilized to quantify the disparities between the detected class and the true class. Therefore, the integration of softmax activation with the cross-entropy loss function is performed to accomplish the classification task. Additionally, the Table 8 shows performance accuracy at 0 dB, with an overall accuracy achieved of 94%. In contrast, the BPSK achieves 100% accuracy, whereas 16−QAM achieves 94%.

The training accuracy of the proposed system in terms of SNR is compared with the Zhou [46], Ali [47], Krzystone [48] and Kim [49] as depicted in the Table 9.

These results indicate that all waveforms perform relatively well at a moderate SNR level (0 dB), with BPSK and QPSK showing the highest accuracy. This suggests that these modulation schemes are more robust to noise compared to others. Similarly, at a lower

Table 9
Comparison of training accuracy vs. SNR.

Accuracy (%) \ SNR (dB)	−20	−15	−10	−5	0	5	10	15
Zhou [46]	14	15	20	35	65	75	83	87
Krzy [48]	13	14	28	34	60	75	82	88
Ali [47]	12	13	20	36	66	77	84	92
Kim [49]	11	12	21	36	65	74	81	93
Proposed	10	14	22	37	67	78	84	94

Table 10
Comparison of time complexity.

Model	Total layers	Parameters	Epocs	Optimizer
Zhou [46]	22	5,71,695	40	SDGM
Krzy [48]	13	27,49,275	72	ADAM
Ali [47]	49	4,27,484	60	ADAM
Kim [49]	22	1,43,760	45	SDGM
Proposed	28	1,41,432	10	ADAM

SNR level (−7 dB), where the noise is more significant, the performance of all waveforms decreases. However, BPSK still achieves perfect accuracy, demonstrating its exceptional robustness to noise. QPSK also performs well with an accuracy of 86%, followed by 64 QAM and 16 QAM. 8 PSK shows the lowest accuracy at this SNR level, indicating it is more noise-resistant.

The computational complexities of the convolutional layer, fully connected layer, and the pooling layer of the proposed system, as well as existing models, can be calculated using the following equations:

$$FLOPs_{(conv)} = 2 \times H_{out} \times W_{out} \times C_{out} \times K_H \times K_w \times C_{in} \tag{22}$$

$$FLOPs_{(FC)} = 2 \times N_{in} \times N_{out} \tag{23}$$

$$FLOPs_{(Pooling)} = H_{out} \times W_{out} \times C_{out} \times K_H \times K_w \tag{24}$$

whereas, H_{out} and W_{out} are the height and width of the output feature map. C_{out} is the number of output channels (filters). K_H and K_w are the height and width of the convolution kernel. C_{in} is the number of input channels. The factor 2 accounts for the multiply and add operations. N_{in} is the number of input neurons and N_{out} is the number of output neurons. In this study, it has been observed that deeper architectures are most effective with more complex datasets. Furthermore, there is a notable relationship between the number of dense layers, the number of neurons, and the dataset complexity. The number of convolutional and dense layers directly impacts the model's runtime. While using lower filter sizes and higher batch sizes can enhance the model's performance, it also increases the computational cost. Additionally, a lower batch size yields better results when the learning rate is low. For models with a greater number of layers, maintaining a lower learning rate leads to improved outcomes as mentioned in the Table 10.

These insights are critical for selecting appropriate waveforms based on the expected noise conditions in communication systems. For scenarios with high noise levels, BPSK and QPSK are preferable due to their robustness and high accuracy. For environments with lower noise levels, more complex modulation schemes like 16 QAM and 64 QAM can be considered to achieve higher data rates while maintaining acceptable accuracy. Figs. 7, and 9 depict the received data in the time domain, frequency domain, and constellation domain, respectively, before the introduction of any channel effects.

The spectrogram image was generated using raw signals modulated with BPSK, QPSK, 8PSK, 16 QAM, and 64QAM, each consisting of 1024 samples per waveform. The central frequency employed for modulation is 902 MHz, and each sample has a duration of 5 ms. Owing to the influence of the channel, a Doppler spread of 5 Hz is observed. This comprehensive representation allows for the analysis of signal characteristics across different modulation schemes under specific channel conditions. The detailed spectrogram provides insights into the temporal and frequency dynamics, offering a valuable resource for understanding the impact of channel effects on various modulation signals as shown in Fig. 8.

Fig. 9 shows the scatter plot image of the received modulated signal, where the x-axis shows the In phase while the y axis shows the quadrature component. These constellations are obtained for $BPSK$, $QPSK$, $8-PSK$, $16-QAM$ and $64-QAM$ at snr −10 dB, −5 dB, 0 dB, 5 dB, 10 dB, and 20 dB respectively.

3.2. Radar performance evaluation

In this section, we will highlight the performance of the Radar receiver. Two targets $\theta_{r_1} = 5^0$ and $\theta_{r_2} = 7^0$ were assumed to be located in far field. The target reflection coefficients were supposed to follow a swirling 2 model which changes from pulse to pulse while remains constant during the entire pulse. ULA having a length of 10 sensors are used at radar receiver array spaced half the wavelength apart. 1000 pulses are used to build data covariance matrix. MUSIC algorithm is used at the radar receiver to perform DOA estimation. The target resolution can be made by [50]

$$|\theta - \theta_i| \leqslant \frac{|\theta_1 - \theta_2|}{2}, i = 1, 2 \tag{25}$$

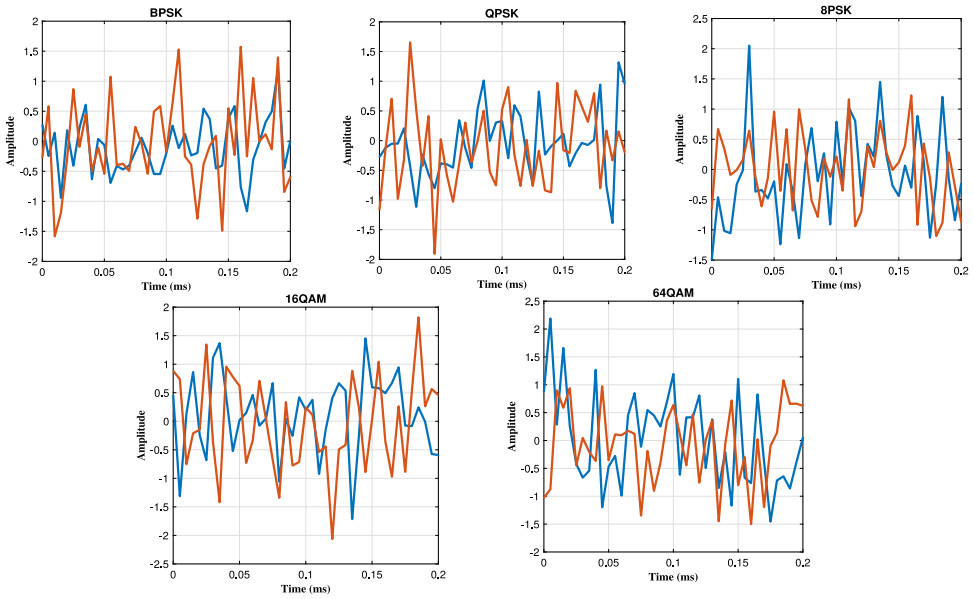

Fig. 7. The I & Q time domain representation of the signal at SNR = 20 dB.

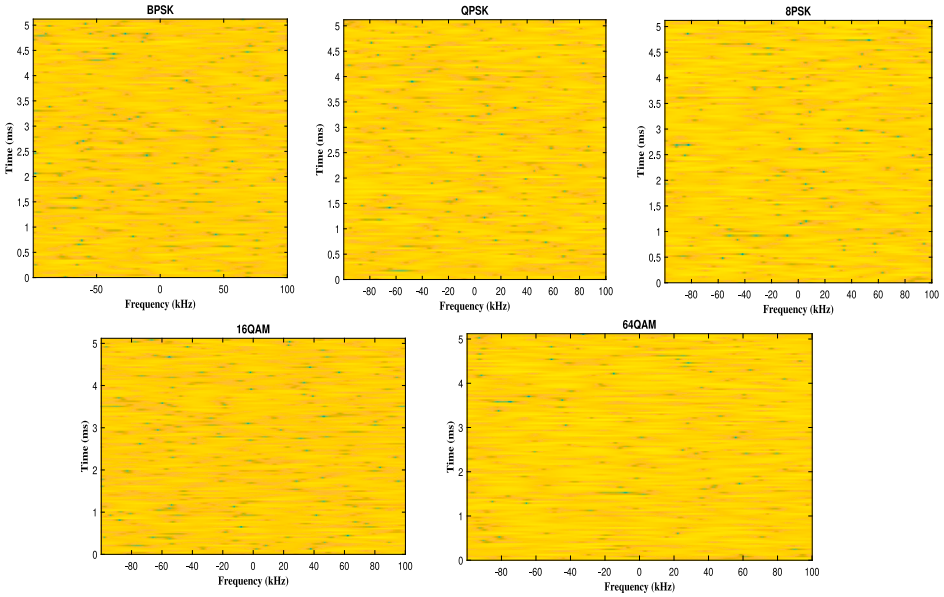

Fig. 8. The spectrogram representation of the signal at SNR = 20 dB. Time is given by the vertical axis while frequency is along the horizontal axis.

Fig. 10 shows the Radar performance when two targets are very close to each other, while Fig. 11 shows the performance of the radar receiver under a high value of SNR.

Moreover, we applied the Friedman test to evaluate the training accuracy of various CNN models across a range of SNR values on the given datasets. The significance of the p-value ($p < 0.005$) was assessed for all models, and the proposed model demonstrated statistical significance, passing all test parameters. For each SNR value, we ranked the performance (training accuracy) of each CNN model. The Friedman test was then used to determine if there were significant differences in performance among the models. The Friedman test statistic (χ_F^2) is calculated using the formula:

$$\chi_F^2 = \frac{12}{nk(k+1)} \sum_{j=1}^{k} R_j^2 - 3n(k+1) \tag{26}$$

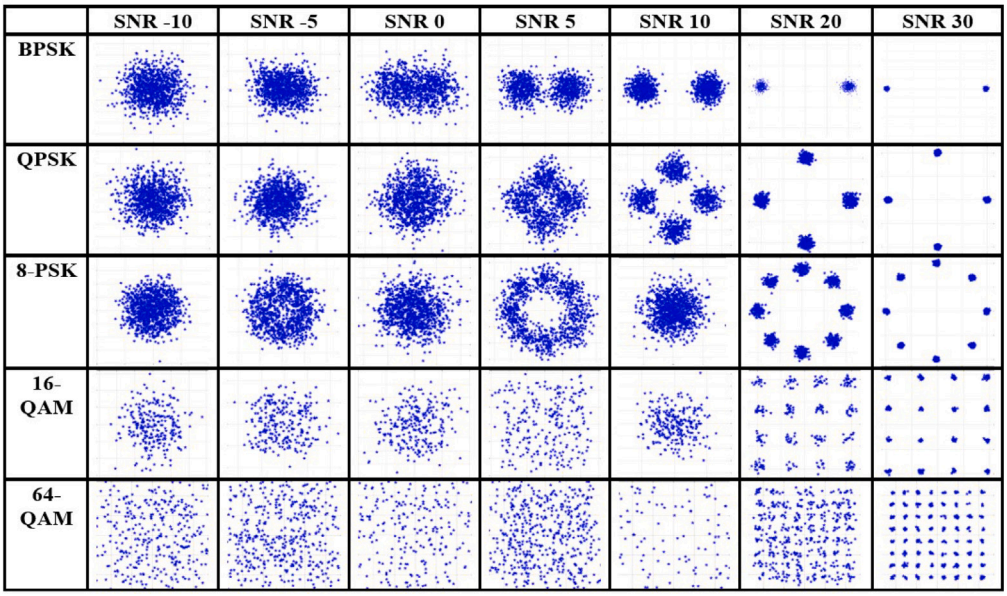

Fig. 9. The Constellation diagrams for digital modulation types of the received signal from SNR = −10 dB to SNR= 30 dB,.

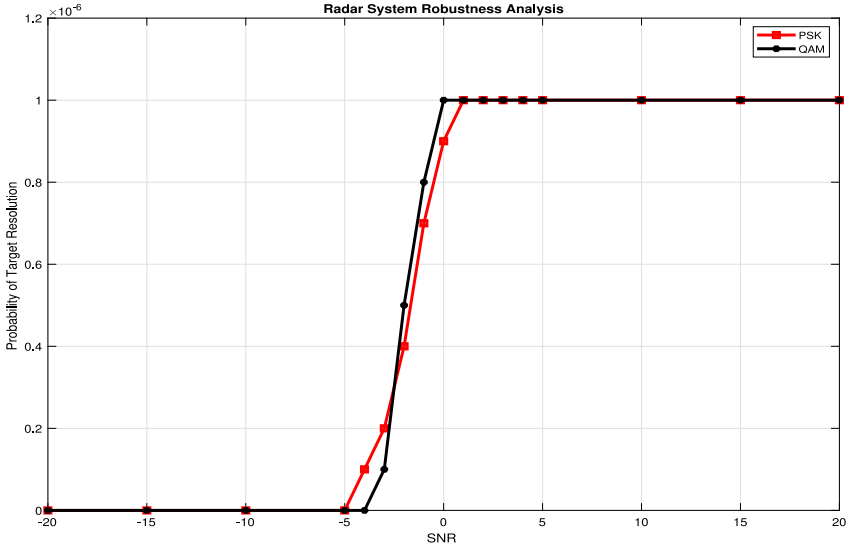

Fig. 10. The Robustness of radar receiver in terms of Target separation vs SNR.

where: n is the number of observations (e.g., different SNR levels), k is the number of groups (e.g., different CNN models), Rj is the sum of ranks for group j. The proposed CNN model showed a statistically significant improvement in training accuracy across the range of SNR values, as evidenced by the Friedman test. The *p*-value was found to be below the threshold for significance, indicating that the proposed model's performance is significantly different from that of the other models tested.

4. Conclusion

In this work, we have presented Cognitive architecture for DFRC for a variety of five communication schemes and two different waveforms. With the aid of deep learning techniques, features are extracted from received signals at the communication receiver. We have simulated its accuracy over a broad range of SNR. In this, a CNN-based image classifier is employed to categorize images depicting various constellation schemes. In comparison with existing modulation classification algorithms for received signals, this CNN-based approach demonstrates superior classification accuracy and avoids the need for manual feature selection. The algorithm exhibits robustness against carrier frequency variations, phase offset, timing errors, and phase jitter. Moreover, this classifier does

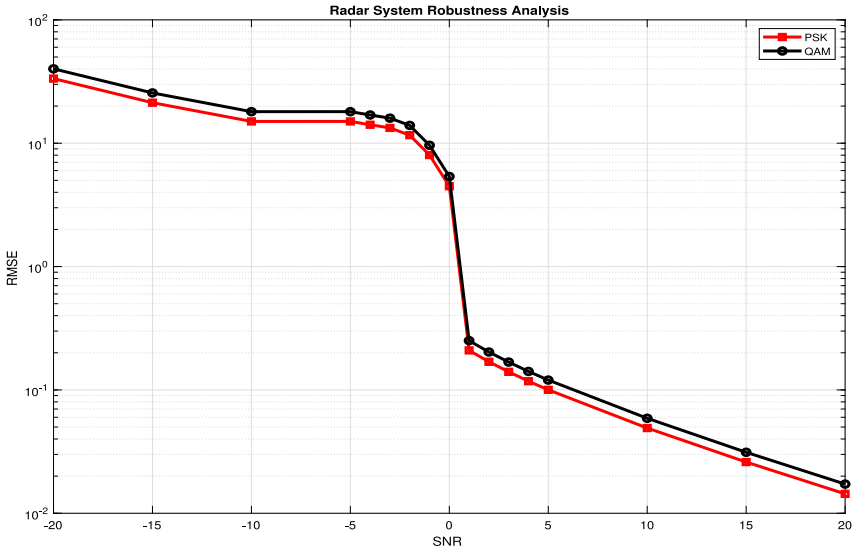

Fig. 11. The Robustness of radar receiver in terms of RMSE and SNR.

not rely on noise variance for classification. Simulations indicate that the proposed CNN-based received signal classification achieves an average classification accuracy above 90.22% and 92.44% for five modulation schemes at −7 dB and 0 dB SNR, respectively.

CRediT authorship contribution statement

Muhammad Fahad Munir: Conceptualization, Methodology, Software, Writing – original draft, Validation. **Abdul Basit:** Project administration, Supervision, Methodology, Conceptualization, Writing – review & editing, Validation. **Wasim Khan:** Supervision, Visualization, Conceptualization, Investigation. **Ahmed Saleem:** Data curation, Writing – original draft. **Aleem Khaliq:** Formal analysis, Data curation. **Nauman Anwar Baig:** Software, Validation, Funding acquisition.

Declaration of competing interest

The authors declare that they have no conflicts of interest to report regarding the present study.

Data availability

Data will be made available on request.

Declaration of Generative AI and AI-assisted technologies in the writing process

During the preparation of this work, the author(s) used ChatGPT 3.5 to partially proofread the introduction part of the manuscript. After using this tool/service, the author(s) reviewed and edited the content as needed and take(s) full responsibility for the publication's content.

Acknowledgments

We are thankful to Robert Gordon University for assistance in publishing this paper.

References

[1] Banafaa M, Shayea I, Din J, Hadri Azmi M, Alashbi A, Ibrahim Daradkeh Y, Alhammadi A. 6G mobile communication technology: Requirements, targets, applications, challenges, advantages, and opportunities. Alexandria Eng J 2023;64:245–74, [Online]. Available: https://www.sciencedirect.com/science/article/pii/S111001682200549X.

[2] Lu S, Liu F, Li Y, Zhang K, Huang H, Zou J, Li X, Dong Y, Dong F, Zhu J, et al. Integrated sensing and communications: Recent advances and ten open challenges. IEEE Internet Things J 2024.

[3] Yadav SS, Hiremath S, Surisetti P, Kumar V, Patra SK. Application of machine learning framework for next-generation wireless networks: Challenges and case studies. In: Handbook of intelligent computing and optimization for sustainable development. Wiley Online Library; 2022, p. 81–99.

[4] Ahmad IAI, Dawodu SO, Osasona F, Akagha OV, Anyanwu AC, Onwusinkwue S. 5G deployment strategies: Challenges and opportunities: A comparative review for africa and the USA. World J Adv Res Rev 2024;21(1):2428–39.

[5] Nawshin F, Gad R, Unal D, Al-Ali AK, Suganthan PN. Malware detection for mobile computing using secure and privacy-preserving machine learning approaches: A comprehensive survey. Comput Electr Eng 2024;117:109233, [Online]. Available: https://www.sciencedirect.com/science/article/pii/S0045790624001617.

[6] Li X, Li J, Liu Y, Ding Z, Nallanathan A. Residual transceiver hardware impairments on cooperative NOMA networks. IEEE Trans Wireless Commun 2020;19(1):680–95.

[7] Munir MF, Basit A, Khan W, Waseem A, Saleem A, Al-Salehi A. Frequency quadrature amplitude modulation based scheme for dual function radar and communication systems. In: 2022 international conference on engineering and emerging technologies. ICEET, 2022, p. 1–5.

[8] Hassanien A, Amin MG, Aboutanios E, Himed B. Dual-function radar communication systems: A solution to the spectrum congestion problem. IEEE Signal Process Mag 2019;36(5):115–26.

[9] Munir MF, Basit A, Khan W, Saleem A, Al-salehi A. A comprehensive study of past, present, and future of spectrum sharing and information embedding techniques in joint wireless communication and radar systems. Wirel Commun Mob Comput 2022;2022.

[10] Eedara IP, Hassanien A, Amin MG. Performance analysis of dual-function multiple-input multiple-output radar-communications using frequency hopping waveforms and phase shift keying signalling. IET Radar Sonar Navig 2021;15(4):402–18.

[11] Tang K, Liao S, Xue Q. Cooperative spectrum sharing in spectrum domain with discrete time energy harvesting for primary user. Ad Hoc Netw 2021;116:102474, [Online]. Available: https://www.sciencedirect.com/science/article/pii/S157087052100041X.

[12] Hassanien A, Amin MG, Zhang YD, Ahmad F. Dual-function radar-communications using phase-rotational invariance. In: 2015 23rd European signal processing conference. EUSIPCO, 2015, p. 1346–50.

[13] Liu F, Masouros C, Petropulu AP, Griffiths H, Hanzo L. Joint radar and communication design: Applications, state-of-the-art, and the road ahead. IEEE Trans Commun 2020;68(6):3834–62.

[14] Wu K, Zhang JA, Huang X, Guo YJ, Heath RW. Waveform design and accurate channel estimation for frequency-hopping MIMO radar-based communications. IEEE Trans Commun 2021;69(2):1244–58.

[15] Du M, Zhong P, Cai X, Bi D, Jing A. Robust Bayesian attention belief network for radar work mode recognition. Digit Signal Process 2023;133:103874.

[16] Zhu Y, Chen M, Wang X, Lin B, Huang H. Synthetic aperture radar image despeckling neural network based on maximum a posteriori probability estimation. Int J Remote Sens 2023;44(2):609–30.

[17] Srivastav A, Mandal S. Radars for autonomous driving: A review of deep learning methods and challenges. IEEE Access 2023.

[18] Iyer S, Velmurugan T, Prakasam P, Sumathi D, Suresh Kumar TR. Support vector machine based spectrum handoff scheme for seamless handover in cognitive radio networks. Concurr Comput: Pract Exper 2023;35(4):e7534.

[19] Liu G, Yang W, Bao Y, Wang Y, Li P. Joint communication and jamming system design based on filter bank multicarrier chirp waveform: Using for curvilinear flight scenario. Remote Sens 2023;15(5):1239.

[20] Baxter W, Aboutanios E, Hassanien A. Joint radar and communications for frequency-hopped MIMO systems. IEEE Trans Signal Process 2022;70:729–42.

[21] Hassanien A, Amin MG, Aboutanios E, Himed B. Dual-function radar communication systems: A solution to the spectrum congestion problem. IEEE Signal Process Mag 2019;36(5):115–26.

[22] Hassanien A, Amin MG, Zhang YD, Ahmad F, Himed B. Non-coherent PSK-based dual-function radar-communication systems. In: 2016 IEEE radar conference. RadarConf, 2016, p. 1–6.

[23] Euzière J, Guinvarc'h R, Lesturgie M, Uguen B, Gillard R. Dual function radar communication time-modulated array. In: 2014 international radar conference. 2014, p. 1–4.

[24] Ahmed A, Zhang YD, Gu Y. Dual-function radar-communications using QAM-based sidelobe modulation. Digit Signal Process 2018;82:166–74, [Online]. Available: https://www.sciencedirect.com/science/article/pii/S1051200418305487.

[25] Krayani A, Alam AS, Calipari M, Marcenaro L, Nallanathan A, Regazzoni C. Automatic modulation classification in cognitive-IoT radios using generalized dynamic Bayesian networks. In: 2021 IEEE 7th world forum on internet of things. WF-IoT, 2021, p. 235–40.

[26] Gupta R, Kumar S, Majhi S. Blind modulation classification for asynchronous OFDM systems over unknown signal parameters and channel statistics. IEEE Trans Veh Technol 2020;69(5):5281–92.

[27] Bibi R, Saeed Y, Zeb A, Ghazal TM, Rahman T, Said RA, Abbas S, Ahmad M, Khan MA. Edge AI-based automated detection and classification of road anomalies in VANET using deep learning. Comput Intell Neurosci 2021;2021:1–16.

[28] Song F, Li Y, Cheng W, Dong L, Li M, Li J. An improved Kalman filter based on long short-memory recurrent neural network for nonlinear radar target tracking. Wirel Commun Mob Comput 2022;2022.

[29] Qiu X, Liu J, Song L, Teng H, Zhang J, Wang Z. A survey of gesture recognition using frequency modulated continuous wave radar. J Comput Commun 2024;12(6):115–34.

[30] Huynh-The T, Luong NC, Phan H, da Costa DB, Pham Q-V. Improved waveform classification for integrated radar-communication 6G systems via convolutional neural networks. IEEE Trans Veh Technol 2024.

[31] Usman M, Lee J-A. AMC-IoT: automatic modulation classification using efficient convolutional neural networks for low powered IoT devices. In: 2020 international conference on information and communication technology convergence. ICTC, IEEE; 2020, p. 288–93.

[32] Kozy M, Yu J, Buehrer RM, Martone A, Sherbondy K. Applying deep-q networks to target tracking to improve cognitive radar. In: 2019 IEEE radar conference. RadarConf, IEEE; 2019, p. 1–6.

[33] Roy C, Yadav SS, Pal V, Singh M, Patra SK, Sinha G, et al. An ensemble deep learning model for automatic modulation classification in 5G and beyond IoT networks. Comput Intell Neurosci 2021;2021.

[34] Zhang X, Wang Y, Huang H, Lin Y, Zhao H, Gui G. Few-shot automatic modulation classification using architecture search and knowledge transfer in radar-communication coexistence scenarios. IEEE Internet Things J 2024.

[35] Kang X, Chen H-m, Chen G, Chang K-C, Clemons TM. Joint detection and classification of communication and radar signals in congested RF environments using YOLOv8. 2024, arXiv preprint arXiv:2406.00582.

[36] Huynh-The T, Hoang V-P, Kim J-W, Le M-T, Zeng M. WaveNet: Towards waveform classification in integrated radar-communication systems with improved accuracy and reduced complexity. IEEE Internet Things J 2024.

[37] Zhang F, Luo C, Xu J, Luo Y, Zheng F-C. Deep learning based automatic modulation recognition: Models, datasets, and challenges. Digit Signal Process 2022;129:103650.

[38] Clement JC, Indira N, Vijayakumar P, Nandakumar R. Deep learning based modulation classification for 5G and beyond wireless systems. Peer-to-Peer Netw Appl 2021;14:319–32.

[39] Ma P, Liu Y, Li L, Zhu Z, Li B. A robust constellation diagram representation for communication signal and automatic modulation classification. Electronics 2023;12(4):920.

[40] Zheng Q, Tian X, Yu Z, Ding Y, Elhanashi A, Saponara S, Kpalma K. MobileRaT: A lightweight radio transformer method for automatic modulation classification in drone communication systems. Drones 2023;7(10):596.

[41] Xiao W, Luo Z, Hu Q. A review of research on signal modulation recognition based on deep learning. Electronics 2022;11(17):2764.

[42] Azari MM, Solanki S, Chatzinotas S, Kodheli O, Sallouha H, Colpaert A, Montoya JFM, Pollin S, Haqiqatnejad A, Mostaani A, et al. Evolution of non-terrestrial networks from 5G to 6G: A survey. IEEE Commun Surv Tutorials 2022;24(4):2633–72.

[43] Proakis JG. Digital communications. McGraw-Hill, Higher Education; 2008, p. 101–7.

[44] Hassanien A, Amin MG, Zhang YD, Ahmad F. Dual-function radar-communications: Information embedding using sidelobe control and waveform diversity. IEEE Trans Signal Process 2015;64(8):2168–81.
[45] Kang J-M, Chun C-J, Kim I-M. Deep learning based channel estimation for MIMO systems with received SNR feedback. IEEE Access 2020;8:121162–81.
[46] Zhou S, Yin Z, Wu Z, Chen Y, Zhao N, Yang Z. A robust modulation classification method using convolutional neural networks. EURASIP J Adv Signal Process 2019;2019:1–15.
[47] Shah AH, Miry AH, Salman TM. Automatic modulation classification based deep learning with mixed feature. Int J Electr Comput Eng (2088-8708) 2023;13(2).
[48] Krzyston J, Bhattacharjea R, Stark A. Complex-valued convolutions for modulation recognition using deep learning. In: 2020 IEEE international conference on communications workshops. ICC Workshops, IEEE; 2020, p. 1–6.
[49] Kim S-H, Kim J-W, Nwadiugwu W-P, Kim D-S. Deep learning-based robust automatic modulation classification for cognitive radio networks. IEEE Access 2021;9:92386–93.
[50] Van Trees HL. Optimum array processing: Part IV of detection, estimation, and modulation theory. John Wiley & Sons; 2002.